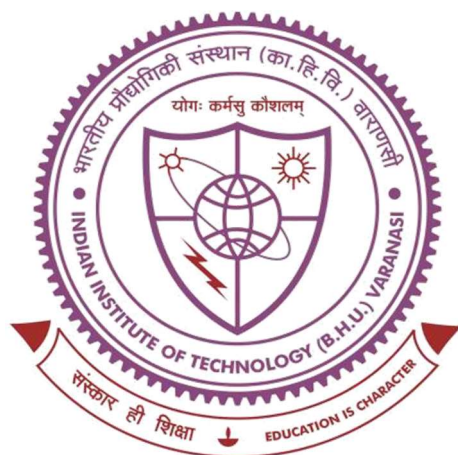


BIOGENIC SYNTHESIS OF NANOSTRUCTURES FOR SENSING, OPTOELECTRONICS, AND THERAPEUTICS



**Thesis submitted in partial fulfillment for the
Award of Degree**

Doctor of Philosophy

By

Ravi Pratap

**DEPARTMENT OF PHYSICS
INDIAN INSTITUTE OF TECHNOLOGY
(BANARAS HINDU UNIVERSITY)
VARANASI – 221005
INDIA**

Roll No- 18171009

Year 2023

CERTIFICATE

It is certified that the work contained in the thesis titled “**Biogenic Synthesis of Nanostructures for Sensing, Optoelectronics, and Therapeutics**” by “**Ravi Pratap**” (Roll No. **18171009**), in partial fulfilment of the requirement for the award of degree of **Doctor of Philosophy** at **Indian Institute of Technology (B.H.U), Varanasi** is a record of her own work carried out under my supervision and guidance, and this work has not been submitted elsewhere for a degree.

It is further certified that the student has fulfilled all the requirements of Comprehensive Examination, Candidacy, and SOTA for the award of Ph.D. Degree.

Date:

Place: Varanasi

(Dr. Avanish Singh Parmar)

Supervisor

Associate Professor,

Department of Physics,

Indian Institute of Technology (BHU),

Varanasi – 221005, (U.P.), India

DECLARATION BY THE CANDIDATE

I, Ravi Pratap (Roll No. 18171009), certify that the work embodied in this thesis is my own bona fide work and carried out by me under the supervision of **Dr. Avanish Singh Parmar** from **25th July 2018** to **21st November 2023** at the **Department of Physics**, Indian Institute of Technology, Varanasi. The matter embodied in this thesis has not been submitted for the award of any other degree/diploma. I declare that I have faithfully acknowledged and given credits to the research workers wherever their works have been cited in my work in this thesis.

I further declare that I have not willfully copied from any other's work, paragraphs, text, data, results, *etc.*, reported in journals, books, magazines, reports, dissertations, thesis, *etc.*, or available at websites and have not included them in this thesis and have not cited as my own work.

Date:

Signature of the Student

(Ravi Pratap)

Place: Varanasi

CERTIFICATE BY THE SUPERVISOR

It is certified that the above statement made by the student is correct to the best of our knowledge.

(Dr. Avanish Singh Parmar)

Supervisor

Associate Professor,

Department of Physics,

Indian Institute of Technology (BHU),

Varanasi – 221005, (U.P.), India

(Prof. Sandip Chatterjee)

Head of Department

Professor,

Department of Physics,

Indian Institute of Technology (BHU),

Varanasi – 221005, (U.P.), India

COPYRIGHT TRANSFER CERTIFICATE

Title of the Thesis: **Biogenic Synthesis of Nanostructures for Sensing,
Optoelectronics, and Therapeutics**

Name of the Student: **Ravi Pratap**

COPYRIGHT TRANSFER

The undersigned hereby assigns to the Indian Institute of Technology (Banaras Hindu University) Varanasi all rights under copyright that may exist in and for the above thesis submitted for the award of the “*Doctor of Philosophy.*”

Date:

Signature of the Student

Place: IIT (BHU), Varanasi

(Ravi Pratap)

Note: However, the author may reproduce or authorize others to reproduce material extracted verbatim from the thesis or derivative of the thesis for author's personal use provided that the source and the Institute's copyright notice are indicated

ACKNOWLEDGMENT

I am deeply grateful for the invaluable support and guidance throughout my Ph.D. journey at the Indian Institute of Technology (Banaras Hindu University), Varanasi. First and foremost, I extend my heartfelt thanks to my supervisor, **Dr. Avanish Singh Parmar**, for his unwavering support, enlightening advice, and immense patience. His dedication to research and his serious approach to life have profoundly influenced my perspective and encouraged my personal growth. His guidance saw me through the challenging phases of my research, laying a strong foundation for my future endeavors. I consider myself fortunate to have had such a compassionate mentor who empowered me to pursue work I deemed important. I also express my gratitude to the members of my Research Progress Evaluation Committee, **Dr. Manoj Kumar** and **Dr. Sunil Kumar Singh**, for their valuable time and feedback during the course of this work. I extend special thanks to **Prof. Sandip Chatterjee**, Head of the Department of Physics, for providing essential resources within the department.

I am thankful to my collaborators, **Dr. Jayeeta Lahiri** (Dept. of Physics, BHU, Varanasi), **Alakh N. Sahu** (Dept. of Pharma, IIT(BHU)), **Prof. Anita K Verma** (Dept. of Zoology, KMC (DU), Delhi), **Dr. Poonam Sharma** (IMS, BHU, Varanasi), and **Shilpi Chaudhary** (PEC, Chandigarh) for the opportunity to collaborate with their labs and for their invaluable insights throughout my Ph.D. work. I extend my gratitude to the Central Instrument Facility Centre and its dedicated staff for providing timely and precise characterization facilities. Their unwavering commitment to maintaining these facilities is truly commendable. I also appreciate the support and valuable suggestions from other esteemed faculty members and research scholars within the department. I am thankful to my lab-mates, **Dr. Devyani Shukla**, **Dr. Kanchan Yadav**, **Dr. Bayazeed Alam**, **Mr. Kaustubh Naik**, **Mr. Shubham Garg**, and **Mr. Saurabh Kumar Srivastava** from whom I gleaned valuable knowledge and with whom I engaged in stimulating

discussions, creating a vibrant lab environment and lots of fun with them. I also extend my thanks to my batch-mates, friends, and juniors for their unwavering support. **Dr. Shiv Kumar Pal, Nurul Hassan, Dr. Puja Kumari** (all from BHU), and **Debadatta Mohapatra, Gaurav Gopal Naik** (IIT-BHU) provided indispensable support during my research journey, and without them, these years would have seemed endless.

I would like to express my deepest gratitude to my parents (**Geeta Devi, Suresh Chandra**) and becoming wife (**Shiv Kumari**) for their unwavering support, love, and encouragement throughout my academic journey. Their sacrifices and belief in my abilities have been the cornerstone of my success. I am also indebted to my siblings, **Anand, Pradeep, Shashi, Vipul, Bittul, Pratiksha, Sandeep, Ranjeet, Bina, Atul** and **Pratik**, for their constant encouragement and understanding during this challenging period.

A special mention goes to my beloved grandparents, **Gangajali** and **Late. Shivdhari Ram**, whose wisdom, love, and blessings have been a source of strength and inspiration for me. Their unwavering belief in my potential has been a guiding light throughout my educational pursuit. I am fortunate to have such a supportive and loving family, and I dedicate this achievement to them.

I greatly acknowledge the **Central Instrumentation Facility center at IIT (BHU), Varanasi**, for providing the facility for various analyses.

Date:

Signature of the Student

Place: IIT (BHU), Varanasi

(Ravi Pratap)

Dedicated
To
My Grand Mother

Table of Contents

CERTIFICATE.....	ii
DECLARATION BY THE CANDIDATE	iii
COPYRIGHT TRANSFER CERTIFICATE	iv
COPYRIGHT TRANSFER	iv
ACKNOWLEDGMENT	v
Table of Contents	viii
List of Figures.....	xii
List of Tables	xviii
List of Abbreviations and Symbols	xix
Preface.....	xxiii
1 Introduction and Literature Review.....	1
1.1 Carbon Nanomaterials.....	1
1.1.1 Fullerene	3
1.1.2 Graphene	4
1.1.3 Carbon Nanotube	5
1.2 Carbon Quantum Dots.....	8
1.2.1 Synthesis Methods of CQDs.....	9
1.2.2 Properties of CQDs	16
1.2.3 Application of CQDs	21
Chapter-2.....	32
2 Methodology and Instrumentation	32
2.1 Materials Used for the Synthesis and Other Experiments of CQDs	32
2.2 Preparation of CQDs	33
2.2.1 <i>Plumeria</i> derived CQDs for Heavy Metal Ions Detection.....	33
2.2.2 <i>Plumeria</i> derived CQDs for WLEDs Application.....	34
2.2.3 Preparation of plant extract and Nanoparticles	35
2.2.4 BN derived CQDs for detection of PNP	36
2.3 Apparatus Used in the Experiments	37

2.4	Experiments Related to CQDs as Detection and Bioimaging.....	38
2.4.1	Selectivity and Sensitivity Measurements	38
2.4.2	Sensing of Hg ²⁺ and As ³⁺ ions	38
2.4.3	In Vitro Cytotoxicity Assay	40
2.4.4	<i>Ex-vivo</i> Hemolysis Assay	40
2.4.5	Fluorescence based assay protocol:	41
2.5	Experiments Related to WLEDs	42
2.5.1	WLEDs Demonstration.....	42
2.6	Experiment Related to GNP as Tumor Regression.....	43
2.6.1	Cell Culture.....	43
2.6.2	Cell cytotoxicity assay	43
2.6.3	Cellular uptake studies	44
2.6.4	<i>in vivo</i> Evaluation of the Nano-formulation (T-Gold, V-Gold, and T+V-Gold) as metastatic Breast Cancer Therapeutic Agent.	45
2.6.5	Histopathological Assessment of Liver section.....	45
2.6.6	Estimation of Nitric Oxide (NO)	46
2.6.7	Estimation of Superoxide dismutase (SOD) activity.....	46
2.6.8	Estimation of lactate dehydrogenase (LDH) release	46
2.6.9	Estimation of Glutathione s-transferase (GST) activity.....	47
2.6.10	Estimation of Reduced GSH activity	47
2.6.11	Statistical Analysis.....	47
Chapter-3	48
3	Biogenic Synthesis of Dual-emission Chlorophyll-rich Carbon Quantum Dots for Detection of Heavy Toxic Metal Ions – Hg (II) and As (III) in Water and Mouse Fibroblast Cell Line NIH-3T3.....	48
3.1	Introduction	48
3.1.1	Source of Water Pollutant.....	48
3.1.2	Techniques for detection of heavy metals in water	50
3.1.3	Properties of CQDs	50
3.2	Results and Discussion.....	52
3.2.1	Optical Characterization of CQDs	52
3.2.2	Sensing of As ³⁺ and Hg ²⁺	61
3.2.3	Quenching and Enhancement Mechanisms	68
3.2.4	Biocompatibility and Bioimaging of CQDs	76

3.3	Conclusion.....	79
Chapter-4.....		81
4 Biogenic Synthesis of Gold Nanoparticles Using Dual Extract of Tulsi-Vinca for Breast Cancer Tumor Regression in Mice.....		81
4.1	Introduction	81
4.1.1	Threat about Triple-Negative Breast Cancer (TNBC).....	81
4.1.2	Treatment of TNBC	81
4.1.3	Meditational properties of Tulsi and Vinca	82
4.2	Results	83
4.2.1	Characterization of GNPs	83
4.2.2	Fourier-transform infrared (FTIR) and XPS Analysis.....	85
4.2.3	XPS Analysis of GNPs	86
4.2.4	Free Radical Scavenging Analysis.....	87
4.2.5	<i>in vitro</i> Cytotoxicity Studies	89
4.2.6	Cellular Uptake Efficiency	90
4.2.7	Tumour Regression Study.....	91
4.2.8	Biochemical Estimations	94
4.3	Discussion	98
4.4	Conclusion.....	107
Chapter-5.....		109
5 Fabrication of White Light Emitting Diodes via High Yield Surface Passivated Carbon Quantum Dots Doped with Terbium		109
5.1	Introduction	109
5.2	RESULTS AND DISCUSSION	111
5.2.1	Optical properties characterization	111
5.2.2	FTIR and XPS measurements.....	113
5.2.3	PL, QY and LT Measurements	116
5.2.4	creation of white LEDs	122
5.2.5	WLEDs Demonstration.....	122
5.3	CONCUSIONS	124
Chapter-6.....		125
6 Fluorometric based detect of organic pollutant of para nitrophenol (PNP) with highly selective and sensitive: using boron nitrate quantum dots (BNQDs)		125

6.1	Introduction	125
6.2	Result and Discussion	127
6.2.1	Optical Characterization of the Synthesized Materials.....	127
6.2.2	Sensitivity and Selectivity of Para Nitro Phenol (PNP).....	135
6.2.3	Sensing of Para Nitro Phenol (PNP).....	137
6.2.4	The Mechanism for PL Quenching.....	143
6.2.5	Real sample analysis	145
6.3	Conclusion.....	148
Chapter-7	150
7	Conclusion and Future Scope.....	150
References	154
List of Publications	189

List of Figures

Figure 1. 1 Allotropes of carbon nanomaterials (Materials, 2021,14, 5978).....	2
Figure 1. 2 Graphene folding to make CNT (<i>Int. J Biological Macromolecules</i> , 2013, 58, 1-6).....	6
Figure 1. 3 Single layered graphene sheet with integer labels (n, m). Types of CNTs knowing the numbers, the diameter and chiral angle may be determined (n, m) (Nanoscale, 2010, 2, 373-380).....	7
Figure 1. 4 (a) Synthesis process and structure of CQDs, (b) Different synthesis techniques of Top-Down and Bottom- Up (Nanomaterials 2021, 11, 3419).....	10
Figure 1. 5 Green synthesis of gold nanoparticles (GNPs) (Molecules, 2022, 27, 1391).	14
Figure 1. 6 (A) synthesis and purification of CQDs (B) CQDs samples under UV-light (365 nm), (C) PL spectra at different wavelength, and (D) Tunable emission spectra of CQDs with different degree of oxidation. (ACS Nano 2016, 10, 1, 484–491).....	18
Figure 1. 7 Various application of carbon quantum dots (CQDs) (Journal of Materials Science, 2021, 56, 1-32).	22
Figure 1. 8 Plumeria leaves extract used for the synthesis of CQDs for the application of metal sensing and bioimaging.....	24
Figure 1. 9 Photos of full-color CQDs and its application in LEDs (A) Photo of d-bCQDs-based LED chip. (B) Photo of o-gCQDs-based LED chip. (C) Photo of p-rCQDs-based LED chip. (D) Photo of wCQDs-based LED chip. (E) CIE chromaticity coordinate of d-bCQDs, o-gCQDs, p-rCQDs, and wCQDs. (F) Emission spectra of the LEDs of d-bCQDs, o-gCQDs, p-rCQDs, and wCQDs (<i>iScience</i> , 2022, 25, 104421).....	25
Figure 1. 10 CQDs-injected mice in vivo fluorescent images. Different excitation wavelengths were used. Red and green indicate CQD and tissue auto-fluorescence, respectively. (RSC Advances 9(12):6460-6481).	28
Figure 1. 11 Microscopic images of E. coli stained with N-CQDs at different concentrations of 0, 500, 1000, 5000ppm (Crystals 2021, Vol. 11, Page 789, 11, 7, 7 2021).....	29
Figure 2. 1 Solvothermal Synthesis of CQDs using Plumeria plant leaves and its applications in metal detection and bioimaging.....	34
Figure 2. 2 Schematic diagram of synthesis and fabrication of WLEDs materials.	35
Figure 2. 3 Schematic diagram of green synthesis method of gold nanoparticles (GNPs) using Tulsi and Vinca plant leaves.	36
Figure 3. 1 (a) UV-Vis Absorption spectra, (b) Emission spectra, (c) FTIR spectra of CQDs prepared at temperature 160°C, and 220°C. (d) C1s, (e) O1s (f) N1s High-resolution XPS photoelectron peaks of CQDs as synthesized at temperature 160°C, and 220°C.	53
Figure 3. 2 Deconvolution of photoelectron XPS peaks with different synthesized temperature. (a), (b), and (c) shows the deconvolution of C1s, O1s, and N1s photoelectron spectra of as synthesized CQDs at 160°C. (d), (e), and (f) shows the deconvolution of C1s, O1s, and N1s photoelectron spectra of as synthesized CQDs at 220°C.	54

- Figure 3. 3** (a) TEM image of CQD160, inset: SAED pattern of CQD160. (b) bar diagram of CQD160 as size distribution. (c) XRD pattern of as synthesized CQD160. (d) Excitation concentration-dependent PL spectra of CQD160 (e) Concentration-dependent PL spectra of CQD160 by using excitation 410nm. (f) TRPL spectra of CQD160.....57
- Figure 3. 4** (a) XPS survey spectra of CQDs as synthesized temperature at 160°C and 220°C. (b), and (c) Shows the concentration dependent excitation spectra of CQDs160 corresponding emission wavelength as 485nm and 676nm.....58
- Figure 3. 5** Stability measurement of CQDs160. (a) measurement of PL emission at different pH value, (b) Bar diagram of pH stability of CQDs160 corresponding 485nm and 676nm. (c) PL emission stability of CQDs160 with respect to storage time. (d) Salinity stability of CQDs160 at different molarity value.....59
- Figure 3. 6** (a) showing the selectivity of metal ions (Hg^{2+} and As^{3+}) using as synthesized CQD160. (b) Bar diagram of metal selectivity by using as synthesized CQD160. (c) showing the selectivity of As^{3+} metal ions using as synthesized CQD220. (d) Bar diagram of metal selectivity by using as synthesized CQD220.60
- Figure 3. 7** Intensity ratio plot of CQD160. (a) F_{676}/F_{485} vs Concentration plot of Hg^{2+} detection. (b) shows the F/F_0 vs concentration graph corresponding 485 nm and 676 nm peaks with addition of Hg^{2+} ions. (c) F_{485}/F_{676} vs Concentration plot of As^{3+} detection. (d) shows the F/F_0 vs concentration graph corresponding 485 nm and 676 nm peaks with addition of As^{3+} ions.61
- Figure 3. 8** (a) PL emission spectra of CQD220 derived by As^{3+} by using excitation wavelength as 410nm, (b) showing the polynomial fitting between F_0/F vs concentration, (c) plotting the linear range of As^{3+} detection and find the LOD value as 9.04nM, (d) PL emission spectra of CQD220 derived by As^{3+} by using excitation wavelength as 350nm, (e) showing the polynomial fitting graph between F_0/F vs concentration, (f) plotting the linear range of As^{3+} detection and find the LOD value as 9.31nM.62
- Figure 3. 9** (a) PL emission-based sensing of Hg^{2+} derived by CQD160 using excitation as 410 nm. (b) F_0/F vs concentration plot of Hg^{2+} from 0 pM to 200 mM. (c) Drawn the linear correlation range of Hg^{2+} ions detection. (d) PL emission spectra of CQD160 derived by As^{3+} by using excitation wavelength as 410nm. (e) The graph between F_0/F vs concentration of As^{3+} from 0 mM to 500 mM. (f) Plotting the linear range of As^{3+} detection.64
- Figure 3. 10** Overlapping study of metal ions (Hg^{2+} and As^{3+}). (a) At fixed concentration of As^{3+} ions with different concentration of the Hg^{2+} ions. (b) Linear fitting of the Hg^{2+} over fixed As^{3+} ions concentration. (c) At fixed concentration of Hg^{2+} ions and varies As^{3+} ions concentration from 10 nM to 100 μ M, (d) showing the linear fitting of the As^{3+} over the fixed concentration of Hg^{2+} ions.66
- Figure 3. 11** Real water sample analysis. (a) and (b) PL emission spectra without and with CQD160 in various real sample using excitation 410nm. (c) and (d) PL emission spectra without and with CQD220 in real water system by exciting wavelength 350nm.68
- Figure 3. 12** (a), (c) TRPL spectra. (b), (d) plot of average lifetime. (e), (f) UV Vis spectra of CQDs(160°C) with added Hg^{2+} and As^{3+} ions respectively.70
- Figure 3. 13** Zeta potential behaviour with metal ions. (a) Zeta potential of synthesized CQDs160 in aqueous medium. (b), and (c) shows the zeta potential of CQDs160 with

Hg ²⁺ (10 μ M) and As ³⁺ (10 μ M). (d) zeta potential of CQDs160 with mixed Hg ²⁺ (10 μ M) and As ³⁺ (10 μ M).....	72
Figure 3. 14 (a) XPS survey spectrum of CQDs160 synthesized with metal ions (As ³⁺ and Hg ²⁺) in range 0 to 1350eV. (b) High resolution XPS spectra of As3d. (c) High resolution XPS spectra of Hg 4f.	73
Figure 3. 15 (a) FTIR analysis of CQD160 prepared with metal ions (As ³⁺ , and Hg ²⁺). (b), (c), and (d) shows the high resolution XPS photoelectron peaks of C1s, O1s, and N1s with metal ions (As ³⁺ , and Hg ²⁺).....	74
Figure 3. 16 Deconvolution of photoelectron XPS peaks with metal As ³⁺ and Hg ²⁺ ions. (a) CQDs160, (b) CQDs160 + As ³⁺ (10 μ M), (c) CQDs160 + Hg ²⁺ (10 μ M) shows the deconvolution of C1s photoelectron spectra. (d) CQDs160, (e) CQDs160 + As ³⁺ (10 μ M), (f) CQDs160 + Hg ²⁺ (10 μ M) shows the deconvolution of O1s photoelectron spectra. (g) CQDs160, (h) CQDs160 + As ³⁺ (10 μ M), (i) CQDs160 + Hg ²⁺ (10 μ M) shows the deconvolution of N1s photoelectron spectra.....	75
Figure 3. 17 (a), and (b) shows the % cytotoxicity and % viability of CQD160 on NIH-3T3 cell line after 24 hrs, 48 hrs and 72 hrs, (c) <i>Ex vivo</i> hemolysis activity of CQD160 after 2 and 4 hrs, (d) fluorescence intensity of CQD160 and CQD160 with As ³⁺ and Hg ²⁺ in NIH-3T3 cell line post 2 hrs of treatment.....	77
Figure 3. 18 Confocal microscopy of control, CQDs, As ³⁺ , Hg ²⁺ , and mixed on pre-treated NIH-3T3 cell line post 2hrs of treatment.	79
Figure 4. 1 (a), (b), and (c) shows the TEM image, inset (a), (b), and (c) shows the SAED pattern of T-Gold, V-Gold, and T+V-Gold. (d) UV-VIS spectra, (e) Emission spectra at fixed excitation 280 nm, (f) XRD patterns, (g) Zeta potential and, (h) DLS of T-Gold, V-Gold, and T+V-Gold nanoparticles (i) FTIR Spectra of T-Gold, V-Gold, and T+V-Gold.....	84
Figure 4. 2 (a) XPS survey spectrum of T-Gold, V-Gold, and T+V-Gold samples, (b) C1s, (c) O1s, (d) Au 4f high resolution XPS photoelectron peaks of T-Gold, V-Gold, and T+V-Gold.....	86
Figure 4. 3 Deconvolution of XPS photoelectron peak spectra. (a) T-Gold, (b) V-Gold, (c) T+V-Gold, deconvolution of C1s XPS spectra, (d) T-Gold, (e) V-Gold, (f) T+V-Gold, deconvolution of O1s XPS spectra, (g) T-Gold, (h) V-Gold, (i) T+V-Gold, deconvolution of Au 4f XPS spectra.....	87
Figure 4. 4 DPPH radical scavenging assay of T-Gold, V-Gold, and T+V-Gold. (a) T-Gold, (d) V-Gold, (g) T+V-Gold UV-VIS absorption spectra of DPPH radical upon a gradual increase of T-Gold, V-Gold, and T+V-Gold, inset shows the photograph of DPPH solution exposed with different concentration of T-Gold, V-Gold, and T+V-Gold. (b), (e), and (h) shows the calibration curve of percentage scavenging of DPPH radicals vs different concentration of T-Gold, V-Gold, and T+V-Gold. (c), (f), (i) shows the linear range of scavenging percentage vs different concentration of T-Gold, V-Gold, and T+V-Gold and calculate the IC ₅₀ value.	88
Figure 4. 5 Cytotoxicity and IC ₅₀ calculation of T-Gold, V-Gold, and T+V-Gold. (a-c) Dose dependent cytotoxicity assay of T-Gold, V-Gold, and T+V-Gold on 4T1 cells for 24hrs,	

48hrs, and 72hrs. (d-f) Dose dependent cytotoxicity assay of T-Gold, V-Gold, and T+V-Gold on NIH-3T3 cells for 24hrs, 48hrs, and 72hrs.	89
Figure 4. 6 (a) Confocal images of cellular uptake of T-Gold, V-Gold, and T+V-Gold by 4T1 metastatic breast cancer cells at different times after feeding T-Gold, V-Gold, and T+V-Gold, Blue is DAPI for labelling the nuclei, green emission from T-Gold, V-Gold, and T+V-Gold. (b) Quantification of the uptake using mean fluorescence intensity of T-Gold, V-Gold, and T+V-Gold in individual cells.	90
Figure 4. 7 The time period from tumour induction to the tumour regression in mice brought on by the nano-formulation (V-Gold, T-Gold and T+V-Gold). The BALB/c Model of 4T1 Mammary Carcinoma was developed, and the effects of IP injections of PBS (1X, pH 7.4), V-Gold (350mg/kg), T-Gold (350mg/kg), and T+V-Gold (350mg/kg) over the period of 21 days post-tumour induction were assessed. The mice were all sacrificed at the same time on day 21, the last day of the experiment. (a) the photograph of the mice's excised breast tumours at day 21 after tumour induction from four groups (n = 4 per group), (b) Graphical evolution of the tumour growth volume in treated mice (from day 10 days after tumour induction to day 21), (c) Weight of excised tumour after treatment with the administered formulation, (d) Body weight of tumour-bearing mice during the course study.	91
Figure 4. 8 (a-c) NO level, (d-f) LDH level, (g-i) SOD level in 4T1 treated mice.....	95
Figure 4. 9 (a-c) GSH level, (d-f) GST level in 4T1 treated mice.	97
Figure 4. 10 Deconvolution of N1s photoelectron XPS spectrum. (a) T-Gold, (b) V-Gold, and (c) T+V-Gold samples.....	100
Figure 4. 11 (a) Dose dependent cytotoxicity of T-Gold, V-Gold, T+V-Gold, and Paclitaxel, (b) Histopathology of the liver section at magnification 40X. Light micrographs of the liver sections from different treatment groups. Normal Control mouse liver section showing normal hepatic architecture of binucleated cells and activated Kupffer cells. The Tumor control, T, V and T+V group didn't show any pathological remarks related to lesions, steatosis and the abundance of micro and macro vesicles in compared to normal control. All the groups showed binucleated cells refer to regeneration.	105
Figure 5. 1 (a) UV-VIS absorption, excitation, and emission spectra of CQDs. (b) UV-vis absorbance of CQDs with various Tb ³⁺ ion molar ratios (inset: The modification of CQDs emission colour under UV light) (c) XRD pattern of CQDs and CQDs + Tb ³⁺ (25%). (d) TEM image of CQDs Inset: Bar graph showing size distribution of CQDs.....	112
Figure 5. 2 Spectroscopic characterisation of CQDs and CQDs+Tb ³⁺ (25%). (a) FTIR spectra with and without Tb ³⁺ ions. High resolution XPS spectra of the photoelectron B.E. peaks at (b) C1s, (c) O1s, and (d) N1s. (e) XPS survey of CQDs and CQDs+Tb ³⁺ (25%). (f) Tb3d spectrum.	114
Figure 5. 3 Deconvolution of C1s, and O1s photoelectron spectra, (a), and (c) for CQDs while (b), and (d) for CQDs+Tb ³⁺ (25%).	116
Figure 5. 4 (a) Excitation dependent study of CQDs in 1-propanol solution. (b) Shows the relation between excitation (350-450 nm) and emission wavelength. (c) PL emission spectra	

of CQDs in 1-propanol solution with different molar ratio of Tb^{3+} ions. (d) QY diagram of CQDs and 25 % Tb^{3+} doped CQDs.	117
Figure 5. 5 The lifetime-decay curves of (a) Plumeria plant leaves, (b) CQDs+ Tb^{3+} (25%) (The laser excitation source is 375 nm). (c) Optical band gap of with and without doped Tb^{3+} (25%) ions. (d) The absorption spectra of undoped and emission spectra of doped Tb^{3+} (25%) ions.....	119
Figure 5. 6 Energy transfer mechanisms from the host CQD to the 4f shell of Tb^{3+} ions, included cross relaxation between $^5D_3 \rightarrow ^5D_4$ and $^7F_6 \rightarrow ^7F_{0,1}$, phonon-assisted non-radiative transition of $^5D_3 \rightarrow ^5D_4$, and radiative transition of $^5D_4 \rightarrow ^7D_j$ ($j = 6, 5, 4, 3$).	121
Figure 5. 7 (a) EL spectrum of the WLEDs with distinct thickness of the CQDs+ Tb^{3+} (25%). Inset: WLEDs demonstration. (b) CIE chromaticity plot for the WLEDs at various molar concentration of Tb^{3+} ions (0%, 5%, 15%, and 25%).....	123
Figure 6. 1 (a) UV-VIS absorption spectra of WH-BN, PNP and WH-BN+PNP, (b) UV-Vis absorption spectra of synthesized BNQDs, PNP and BNQDs + PNP, (c) Tau plot of WH-BN, (d) Tau plot of synthesized BNQDs.....	128
Figure 6. 2 (a) FTIR spectra of PNP, BNQDs, and BNQDs + PNP, (b) XRD spectra of the BNQDs, PNP, and BNQDs + PNP, (c) Zeta potential of BNQDs, PNP, and mixed of BNQDs +PNP, (d) XPS survey spectra of BNQDs, PNP, and BNQDs +PNP.	129
Figure 6. 3 (a, b, & c) High resolution XPS photoelectron peaks of C1s, O1s, and N1s of the BNQDs, PNP, and BNQDs + PNP. (d) High resolution XPS photoelectron peaks of B1s of the BNQDs, and BNQDs + PNP.	131
Figure 6. 4 (a, b, & c) C1s deconvolution of BNQDs, PNP, and BNQDs + PNP, (d, e, & f) shows the XPS photoelectron deconvolution of O1s BNQDs, PNP, and BNQDs + PNP. ...	133
Figure 6. 5 Deconvolution of XPS spectra, (a) High resolution of photoelectron XPS spectra recorded between 0 to 1350eV, (b, & c) shows the deconvolution of B1s photoelectron XPS spectra of BNQDs with and without PNP, (d-f) shows the deconvolution of N1s of BNQDs, PNP, and BNQDs + PNP.	134
Figure 6. 6 (a) PL emission spectra of control (BNQDs) and BNQDs with different metal ions by using excitation wavelength 340nm, (b) Bar diagram of the PNP detection with respect to different metal ions, (c) PL emission spectra of control (BNQDs) and BNQDs with different PNP type similar molecules by using excitation wavelength 340nm, (d) Bar diagram of the PNP detection with respect to similar molecules.	136
Figure 6. 7 PL emission Stability study of BNQDs, (a) Study of PL emission stability at different pH value, (b) PL emission stability of BNQDs in the presence of exposing UV light at different times, (c) PL emission stability of BNQDs at different concentration of salinity, (d) shows the time of sample storage study of BNQDs.....	137
Figure 6. 8 (a) PL emission spectra of BNQDs with different concentration of PNP (0pM- 100 \square M), (b) Stern-Volmer plot, inset shows the linear fitting in the range 0.1nM to 1 \square M, (c) Lineweaver-Burk plot of PL quenching with the addition of different concentration of PNP, (d) Modified S-V plot for the sensing of PNP.	139

Figure 6. 9 (a- d) TRPL spectra of as synthesized materials BNQDs with and without PNP at different concentration (100nM, 500nM, and 1 μ M) with correlation coefficient ($R^2 = 0.992$), excitation and emission fixed at 370nm and 425nm..... 141

Figure 6. 10 Plot of lifetime ratio plot of BNQDs with addition of PNP, (a) shows the average lifetime decay curve, (b) calibration plot of lifetime decay for τ_1 and τ_2 143

Figure 6. 11 Fluorimetry based real samples testing in pesticides and some water system using excitation as 340nm, (a) PL emission spectra of different pesticides at same concentration (100 μ l) in DI, (b) PL emission spectra of pesticides in the presence of BNQDs, (c) PL emission spectra of different pesticides with PNP in the presence of BNQDs, (d) PL emission spectra in the presence of real water system, (e) PL emission spectra of real water system in the presence of BNQDs, (f) PL emission spectra of real water system with PNP in the presence of BNQDs. 146

Figure 6. 12 Overlapping study of PNP with similar molecular structure molecules, (a) PL emission spectra of BNQDs with aniline, aminophenol, dinitrobenzene, methyl phenol, and phenol, (b-e) shows the overlapping PL emission spectra of PNP with aniline, aminophenol, dinitrobenzene, methyl phenol, and phenol. 147

List of Tables

Table 1. 1 Various Forms of Biomass Serve as Carbon Precursors for CQD Synthesis and applications.	12
Table 3. 1 (a), and (b) The C1s, O1s peak positions obtained after peak fitting. The error ± 0.2 eV for peak C1s and O1s peak of CQDs at different synthesis temperature.	56
Table 3. 2 LOD comparison of Hg ²⁺ and As ³⁺ ions with the other literature reported system.	64
Table 3. 3 (a), and (b) Decay time of CQDs160 with and without addition of Hg ²⁺ and As ³⁺ ions.	71
Table 3. 4 Deconvolution of Different functional groups of (a) C1s, (b) O1s, and N1s.	76
Table 4. 1 (a) Tumor Regression, (b) Tumor weight, (c) Body Weight Study of T, V, and T+V-Gold.	94
Table 4. 2 (a) NO assay, (b) LDH assay, (c) SOD assay data for oxidative stress are represented as mean \pm stdev with n=4, in different tissue samples.	96
Table 4. 3 (a-c) GSH level, (d-f) GST level in 4T1 treated mice.	97
Table 4. 4 (a) Atomic percentage of C1s, O1s, N1s, and Au 4f of T-Gold, V-Gold, and T+V-Gold, (b) Area% of functional groups present in C1s, O1s, N1s, and Au4f of T-Gold, V-Gold, and T+V-Gold.	101
Table 4. 5 Containing IC ₅₀ dose of T-Gold, V-Gold, T+V-Gold, and Paclitaxel against 4T1 metastatic breast cancer.	103
Table 6. 1 The C1s, O1s, N1s, and B1s peak positions and their atomic percentage of the synthesized BNQDs, PNP, and BNQDs + PNP.	132
Table 6. 2 Table comparing the LOD limit of PNP detection using different active sensing material.	138
Table 6. 3 Decay time of BNQDs in presence of different concentration of PNP.	142
Table 6. 4 (a) (b) The C1s, O1s peak positions obtained after peak fitting. The error ± 0.2 eV for peak C1s and O1s peak with PNP.	145

List of Abbreviations and Symbols

D	Dimensional
CVD	Chemical Vapour Deposition
AFM	Atomic Force Microscopy
TEM	Transmission Electron Microscopy
SEM	Scanning Electron Microscopy
HRTEM	High Resolution Transmission Electron Microscopy
XRD	X-ray diffraction
ITO	Indium Tin Oxide
FLG	Few-layered Graphene
nm	Nanometre
m ² /g	Meter Square Per Gram
GO	Graphene Oxide
OH	Hydroxide
-O-	Epoxide
FRET	Förster Resonance Energy Transfer
CQD	Carbon Quantum Dot
PL	Photoluminescence
λ	Wavelength
UV	Ultraviolet
CdTe	Cadmium Telluride
ZnSe	Zinc Selenide
PbS	Lead Sulphate
CL	Chemiluminescence
ECL	Electrochemical Luminescence
UCPL	Up-conversion Photoluminescence
PET	Photoinduced Electron Transfer
CNT	Carbon Nanotube
SWCNT	Single Walled Carbon Nanotube
MWCNT	Multi walled Carbon Nanotube
HOMO	Highest Occupied Molecular Orbital

LUMO	Lowest Unoccupied Molecular Orbital
NIR	Near Infra-red
AIEE	Aggregation Induced Emission Enhancement
AIEQ	Aggregation Induced Emission Quenching
SQE	Static Quenching Effect
DQE	Dynamic Quenching Effect
ET	Energy Transfer
CND	Carbon Nano Dot
GQD	Graphene Quantum Dot
PD	Polymeric Dot
PEG	Poly Ethylene Glycol
QY/ \emptyset	Quantum Yield
ZnO	Zinc Oxide
M Ω .cm	Mega Ohm. Centimeter
DMSO	Dimethyl sulfoxide
HCl	Hydrochloric Acid
NaCl	Sodium Chloride
CaCl ₂	Calcium Chloride
CdSO ₄	Cadmium Sulfate
ZnCl ₂	Zinc Chloride
Ag(NO ₃)	Silver Nitrate
Pb(NO ₃) ₂	Lead Nitrate
SnCl ₂	Stannous Chloride
kV/eV	Kilo Volts/Electron Volts
PL	Photoluminescence
I/A/ η	Intensity/Absorbance/Refractive Index
R	Reference
DPPH	2,2-diphenyl-1-picrylhydrazyl 3-(4,5-dimethylthiazol-2-yl)-2,5-diphenyl tetrazolium
MTT	bromide
μ g/L	Micro Gram per Litre
A	Absorbance
-CN	Cyano

-COOH	Carboxylic
nM	Nano Molar
pM	Pico Molar
AuNP	Gold Nanoparticle
AgNP	Silver Nanoparticle
FTIR	Fourier Transform Infrared Spectroscopy
EPA	Environmental Protection Agency
NCCS	National Centre for Cell Science, Pune
DMEM	Dulbecco's Modified Eagle Medium
MEM	Minimum Essential Medium
IC50	Half Maximal Inhibitory Concentration
ROS	Reactive Oxygen Species
RFI	Relative Fluorescence Intensity
DAPI	4',6-diamidino-2-phenylindole
ETL	Electron Transport Layer
HTL	Hole Transport layer
EL	Emissive Layer
LED	Light-emitting Diode
OLED	Organic Light Emitting Diode
OLET	Organic Light Emitting Transistor
BNQDs	Boron nitride quantum dots
OSC	organic solar cells
DLS	Dynamic Light Scattering
XPS	X-ray Photoelectron Spectroscopy
SAED	Selected Area Electron Diffraction
(C=O), C-O	Carboxyl, Carbonyl
C-H, C=C	Carbon Bonds
τ_{avg}	Average Photoluminescence Lifetime
(F ₀ /F)	Relative Fluorescence Response
K _{sv}	Stern–Volmer Quenching Constant
C	Concentration of the Quencher
LOD	Limit of Detection
LSPR	Localized Surface Plasmon Resonance

ECQD/WCQDs	Ethanol-based and Water-based Carbon Quantum Dots
SPB	Surface Plasmon Band
WHO	World Health Organization
ppb	parts per billion
DI	Deionized Water
DW	Dry weight
T ₅₀	Half Life
MD	Molecular Dynamics
PEDOT: PSS	Poly3,4ethylenedioxythiophene: polystyrenesulfonate
PFO	Polyfluorene
PSBF	Polyspirobifluorene
ODA	Octadecylamine
LDH	Lactate Dehydrogenase
DCB	Dichlorobenzene

Preface

Carbon nanomaterials have gradually attracted the attention of the scientific community and emerged as new valuable materials. Carbon, one of the most abundant substances on Earth, and its allotropes such as fullerenes, carbon nanotubes, graphene and carbon quantum dots have been proposed for energy generation, sensing, bio-imaging and drug delivery in the past two decades due to their extraordinary properties and ease of fabrication. Carbon quantum dots (CQDs) are considered zero-dimensional materials (with a diameter as small as 10 nm) with enhanced optical and electronic properties such as intense fluorescence, high electron mobility, biocompatibility and high stability. Since their accidental discovery in 2004 during the purification of single-walled nanotubes, CQDs have been intensively researched over the last two decades and used in numerous fields. Compared to semiconductor quantum dots, CQDs consist mainly of a carbonaceous core, which makes them biocompatible and non-toxic. They can be used as biomarkers, metal sensors, optical sensors, light-harvesting material, fluorescent ink, anti-cancer agents and, due to the low-cost precursor material, also as potential drug carriers. Several studies have shown that CQDs can be produced at high temperature and high pressure from different precursor materials while maintaining similar photophysical properties. It would be beneficial to further investigate the optical and electronic properties of CQDs. The morphology of CQDs has been well studied in terms of their size and shape. Although the study of nanostructured carbon materials has experienced rapid development and remains an active research topic, there is still a lack of fundamental understanding of the growth mechanisms and the essential elements responsible for the synthesis of CQDs. Carbon-based nanomaterials are currently considered a milestone in nanotechnology as they drive scientific progress and have numerous industrial applications. In this work, different strategies for the synthesis and use of carbon nanomaterials in sensing, bio-imaging and optoelectronic systems are discussed. The synthesis methods for carbon quantum dots have been studied in detail using various

spectroscopic and microscopic techniques. For the synthesis of CQDs, different plant leaves were used as starting materials and water and ethanol as solvents at different temperatures depending on the application.

This thesis also investigates the applications of CQDs in sensing and bio-imaging. We demonstrate that the optical and morphological properties of CQDs can be tuned by varying the hydrothermal synthesis temperature from 120°C to 220°C. We have functionalized CQDs with chlorophyll utilizing chlorophyll-rich *Plumeria* leaves in ethanol as a carbon source because chlorophyll dissolves easily in ethanol which is less hazardous than other organic solvents. CQDs synthesized at 160°C can be used as a dual probe sensor for the selective detection of Hg⁺ ions and As³⁺ ions with lower detection limits. In another study, gold nanoparticles (GNP) were synthesized with *Tulsi* and *Vinca* extracts exhibiting different shapes and sizes with enhanced crystallinity. The T+V gold nanoformulation exhibited superior cytotoxicity against breast cancer cells (4T1) *in vitro* and showed remarkable tumor regression in a mouse model. The anti-cancer potential was attributed to the release of anti-cancer metabolites and alterations in antioxidant metabolic pathways, as evidenced by the modulation of glutathione family enzymes and oxidative stress markers. The T+V gold nanoformulation exhibited negligible toxicity in normal cells and organs, highlighting its potential as an effective and safe therapeutic agent. In a separate study, fluorescent functionalized carbon quantum dots (CQDs) were synthesized by a hydrothermal method using *Plumeria* plant leaves and Tb³⁺ ions as a surface passivator. The doped CQDs exhibited excitation-dependent photoluminescence with strong peaks attributed to Tb³⁺ doping. In combination with a UV chip, the CQDs exhibited efficient white light emission, making them promising candidates for white light emitting diodes (WLEDs). The resulting WLEDs had the desired color coordinates, color temperatures and a high color rendering index (CRI). Finally, boron nitride quantum dots (BNQDs) were synthesized from boron nitrate

nano powder through a hydrothermal process. The BNQDs exhibited excellent sensing behavior towards p-nitrophenol (PNP) with a low detection limit of about 7.91 pM. Time-resolved photoluminescence studies confirmed the high selectivity and sensitivity of the BNQDs for PNP sensing. The cost-effective and environmentally friendly synthesis approach presented in this study contributes to the development of nanomaterial-based sensing technologies with potential applications in environmental monitoring. Overall, our versatile approach in the synthesis and characterization of nanomaterials demonstrates their versatility for sensing and therapeutic applications and highlights their potential impact on various scientific and technological fields.